AFRL-OSR-VA-TR-2013-0583

Wavelength-Tunable IR Detector based on Suspended Bilayer Graphene Micro Ribbons

EUI-HYEOK YANG

STEVENS INSTITUTE OF TECHNOLOGY

11/05/2013
Final Report

AIR FORCE RESEARCH LABORATORY
AF OFFICE OF SCIENTIFIC RESEARCH (AFOSR)/RSE
ARLINGTON, VIRGINIA 22203
AIR FORCE MATERIEL COMMAND

REPORT DOCUMENTATION PAGE

Form Approved
OMB No. 0704-0188

1. REPORT DATE *(DD-MM-YYYY)*	**2. REPORT TYPE**	**3. DATES COVERED** *(From - To)*
11/05/2013	Final Performance Report	7/1/2012 - 6/30/2013

4. TITLE AND SUBTITLE

Wavelength-Tunable IR Detector based on Suspended Bilayer Graphene Micro Ribbons

5a. CONTRACT NUMBER
N/A

5b. GRANT NUMBER
FA9550-12-1-0326

5c. PROGRAM ELEMENT NUMBER
N/A

6. AUTHOR(S)

Yang, Eui-Hyeok
Strauf, Stefan
Patil, Vikram
Kumar, Kitu

5d. PROJECT NUMBER
N/A

5e. TASK NUMBER
N/A

5f. WORK UNIT NUMBER
N/A

7. PERFORMING ORGANIZATION NAME(S) AND ADDRESS(ES)

Stevens Institute of Technology
One Castle Point on Hudson
Hoboken, NJ 07030

8. PERFORMING ORGANIZATION REPORT NUMBER
N/A

9. SPONSORING / MONITORING AGENCY NAME(S) AND ADDRESS(ES)

US Air Force Office of Scientific Research (AFOSR)
875 North Randolph Street, Room 3112
Arlington, VA 22203

10. SPONSOR/MONITOR'S ACRONYM(S)
USAF, AFRL

11. SPONSOR/MONITOR'S REPORT NUMBER(S)
N/A

12. DISTRIBUTION / AVAILABILITY STATEMENT

Approved for public release; distribution is unlimited

13. SUPPLEMENTARY NOTES

N/A

14. ABSTRACT

The original goal of this three-year project was to investigate bandgap-tunable bilayer-graphene microribbons allowing continuously tunable photodetection in the IR bands. Due to the government sequestration, the 2nd and 3rd years increments toward this project have been defunded. Here we are using our 1st year result as our final performance report. To this end we designed, fabricated, and characterized in Year One a device with suspended graphene microribbons, and found that fully suspended CVD-grown graphene devices are dominated by the photoelectric effect, which is promising towards CVD-grown graphene photodetectors approaching THz cut-off frequencies.

15. SUBJECT TERMS

chemical vapor deposition, strain tuning, bandgap-tunability, suspended graphene, microribbons, photodetector, THz cut-off freq

16. SECURITY CLASSIFICATION OF:			**17. LIMITATION OF ABSTRACT**	**18. NUMBER OF PAGES**	**19a. NAME OF RESPONSIBLE PERSON**
a. REPORT	**b. ABSTRACT**	**c. THIS PAGE**	UU	11	Eui-Hyeok Yang
U	U	U			**19b. TELEPHONE NUMBER** *(include area code)* 201-216-5574

AFOSR Final Performance Report

Grant Title: Wavelength-Tunable IR Detector based on Suspended Bilayer Graphene Micro Ribbons

Grant No.: FA9550-12-1-0326

Reporting Period: 1 July 2012 to 30 June 2013

Program Manager:
Dr. Gernot Pomrenke
Program Officer
Air Force Office of Scientific Research
Arlington, VA 22203-1768
Tele: (703) 696-8426
DSN: 426-8426
FAX: (703) 696-8481
Email: gernot.pomrenke@us.af.mil

Principal Investigator:
Prof. Eui-Hyeok Yang
Stevens Institute of Technology
Castle Point on the Hudson, Hoboken, NJ 07030
(201) 216-5574
E-mail: eyang@stevens.edu

1. Project Summary

The original goal of this three-year project was to investigate bandgap-tunable bilayer-graphene microribbons allowing continuously tunable photodetection in the IR bands (**Figure 1**). *Due to the government sequestration, the 2nd and 3rd years increments toward this project have been defunded. Here we are using our 1st year result as our final performance report.*

The approach was to suspend graphene such that it can be actuated, thereby opening a variable bandgap. While most work on graphene photodetectors was done with tiny exfoliated flakes, we developed a scalable approach using chemical vapor deposition (CVD) grown graphene and studied the lesser known photophysics in CVD material. To this end we designed, fabricated, and characterized in Year One a device with suspended graphene microribbons. The CVD growth was optimized and large-area graphene transferred onto a wafer with a sacrificial layer. During this optimization, we have discovered a new growth mode of two-lobed symmetrical curvilinear graphene domains. After optimization the CVD material quality was evaluated with Raman spectroscopy and optical transmission and was found to be either monolayer or bilayer with minimal defect density. The photoresponse from fabricated photodetectors was measured before and after it was suspended in order to avoid effects from spatial inhomogeneity in the CVD material. We have demonstrated four-fold enhancement of the photoresponsitivity, with best values up to 0.4 mA/W, in fully suspended CVD-grown graphene photodetector devices over substrate-supported graphene. In addition, we have shown that the light-current input/output curves give valuable information on the underlying photophysical process responsible for the generated photocurrent. Finally, we have found that fully suspended CVD-grown graphene devices are dominated by the photoelectric effect, which is promising towards CVD-grown graphene photodetectors approaching THz cut-off frequencies. Based on these promising and significant results, our original goals in Years Two and Three were to tackle the actuation of the suspended graphene microribbon and the wavelength scanning capabilities of the photodetector.

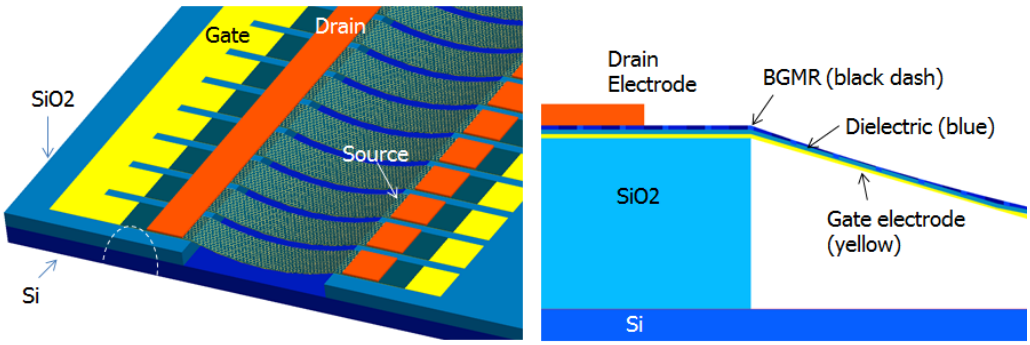

Figure 1: Conceptual schematic of an electrostatically actuated suspended bilayer graphene microribbon (BGMR) array for bandgap tuning with the strain gate and one of the two electrodes required to induce lateral electrical fields. The electrode under the BGMR is used for both photocurrent and electrical bandgap tuning (top electrode not shown for clarity). The arrays of BGMRs are arranged with carefully chosen dimensions, ensuring continuous detection of radiation over a broadband spectrum in the IR regime.

2. Technical Results

2.1 The graphene domains grown on copper at atmospheric pressure using chemical vapor deposition: We demonstrated the chemical vapor deposition (CVD) growth of two-lobed symmetrical curvilinear graphene domains specifically on Cu{100} surface orientations at atmospheric pressure (**Figure 2**). We utilized electron backscattered diffraction, scanning electron microscopy and Raman spectroscopy to determine an as-yet unexplored growth mode producing such a shape and demonstrated how its growth and morphology are dependent on the underlying Cu crystal structure especially in the high CH4:H2 regime. We showed that both monolayer and bilayer curvilinear domains are grown on Cu{100} surfaces; furthermore, we showed that characteristic atmospheric pressure CVD hexagonal domains are grown on all other Cu facets with an isotropic growth rate which is more rapid than that on Cu{100}. These findings indicate that the Cu-graphene complex is predominant mechanistically at atmospheric pressure, which is an important step towards tailoring graphene properties via substrate engineering.

2.2 The Effect of the Thermal Annealing on PMMA-transferred Graphene: The impact of polymer removal by forming gas and vacuum annealing on the doping, strain, and morphology of chemical vapor deposited (CVD) and mechanically exfoliated (ME) graphene was investigated using Raman spectroscopy and atomic force microscopy (AFM) (**Figure 3**). The behavior of graphene exposed and unexposed to polymer was compared. It is found that the well-known doping effect after forming gas annealing is induced in graphene by polymeric residue/H-functionalization. Further, forming gas annealing of ME graphene was shown to induce strain via pinning of the graphene layer to the substrate. It was found that vacuum annealing removes most polymeric residue, with minor doping and strain effects. Finally, a study of AFM step height and roughness measurements provides now a comprehensive understanding of those annealing-based processes which create morphological changes and directly influence doping and strain in the graphene layer, such as removal of polymer, removal of the interfacial graphene-substrate water layer, environmental doping effects and deformation of the graphene layer.

2.3 Photocurrent Sensing with CVD Graphene Microribbons: Large area graphene was grown on high purity copper foil using a low pressure CVD furnace at 1000 ^{o}C in a hydrogen, argon and methane environment. Raman spectrum of the graphene transferred onto 300 nm SiO_2 substrate confirms good quality monolayer graphene film (For more details see supporting online information.). The graphene was then etched into ribbons using reactive ion etching with O_2. The patterned graphene microribbons were then contacted with e-beam evaporated 125 nm thick Ti/Au contact pads, defined by the liftoff method using e-beam lithography of PMMA resist and lifted off by N-Methyl-2-pyrrolidone (NMP). The devices were then wire bonded using 25 μm thick Au wires on a chip carrier for electrical measurements. For suspending graphene, we etched the 300nm thick underlying layer of SiO_2 using (6:1) buffered oxide etchant (BOE) followed by critical point drying (CPD) to avoid damage to the suspended graphene ribbon.

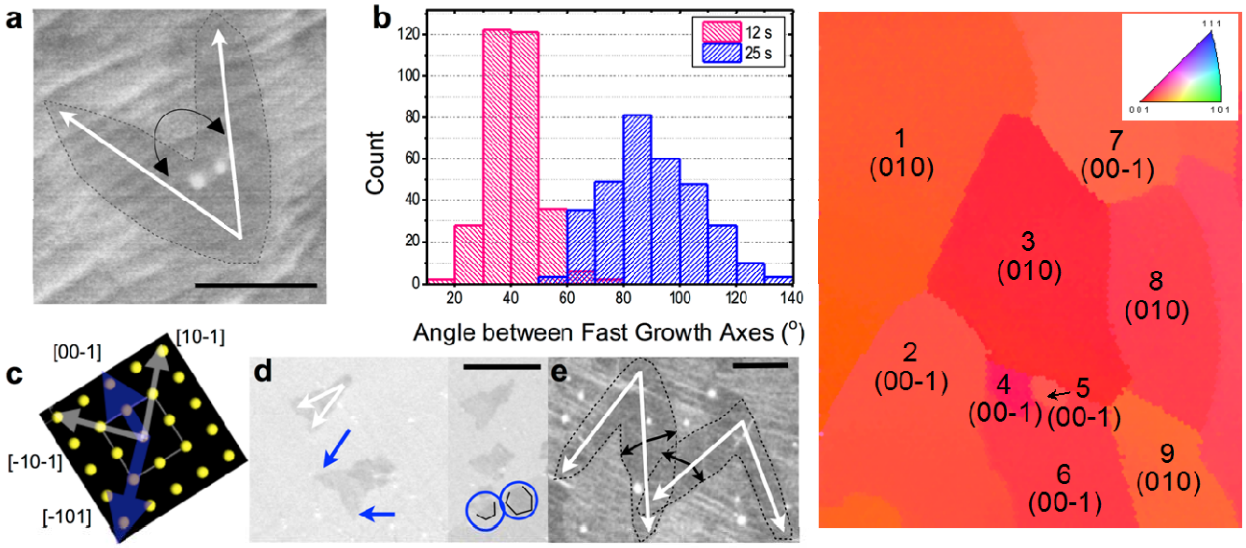

Figure 2: Two-lobed symmetrical curvilinear graphene domains specifically on Cu{100} surface orientations; its growth and morphology are dependent on the underlying Cu crystal structure

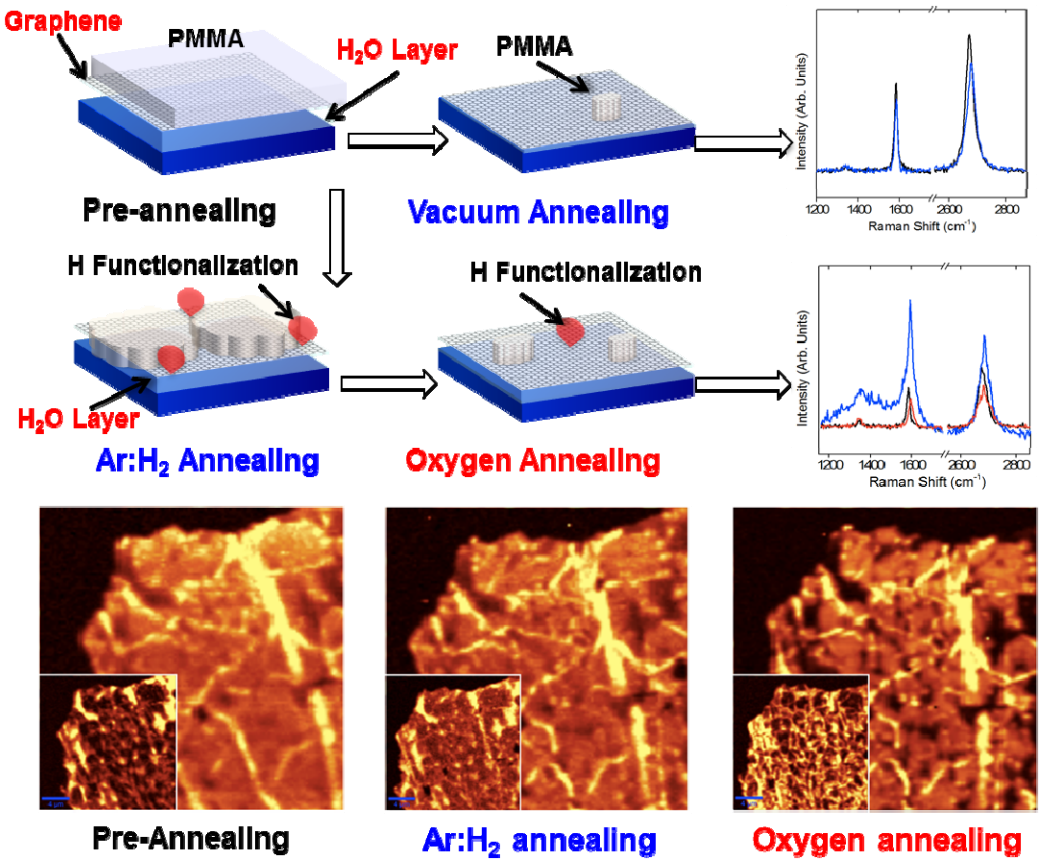

Figure 3: Annealing-based processes create morphological changes and directly influence doping and strain

All the measurements were performed at room temperature in a chamber with vacuum level of 10^{-6} mbar. The photoresponse of the graphene ribbons was measured using a lock-in amplifier by positioning a 532 nm wavelength laser spot onto the ribbon. A spot of approximately 1 μm diameter (FWHM) was focused using a 50x objective with working distance of 13 mm. The position of the laser spot was manipulated by using piezoelectric motor controlled scanning mirrors with nanometer precision in X and Y directions. The incident laser power, which was measured to be 20 mW at maximum, was controlled by using neutral density filters to sweep between 1 nW and 2.8 mW. The beam was modulated with a chopper wheel at 2 kHz. All current and voltage values were supplied by two Keithly 2400 source meters, while output was read from the lock-in amplifier. A moderate source-drain bias of 0.1 V was used for photocurrent measurements. Back-gate sweeps were performed with 1mV with voltage ranges selected to center the Dirac point.

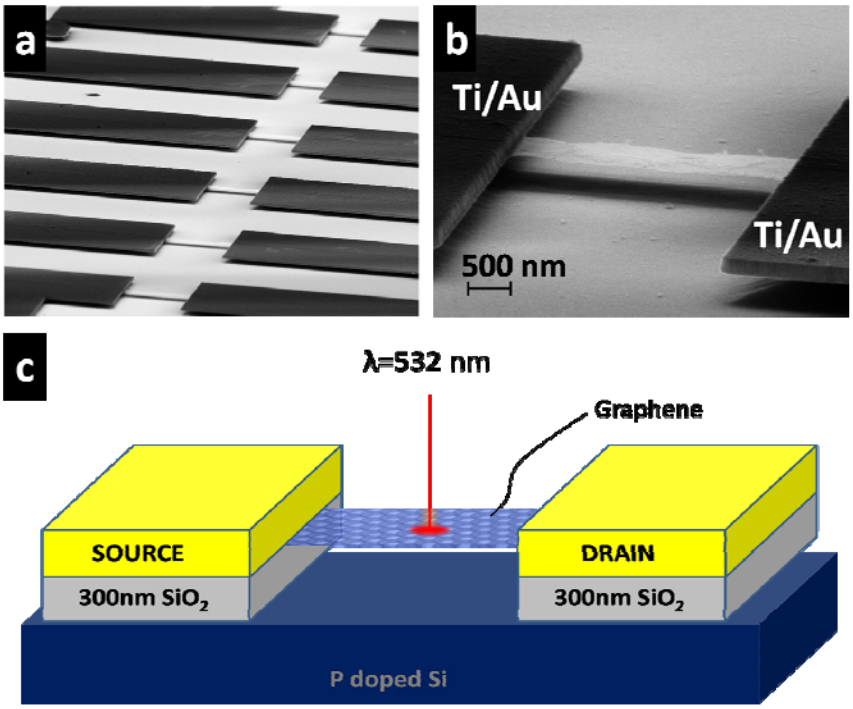

Figure 4. **CVD-grown graphene photodetector devices.** (**a**) SEM images showing an array of fully suspended graphene photodetectors fabricated on large area CVD graphene on a 300nm layer of SiO_2thermally grown on p-type silicon substrate. (**b**) SEM image of individual photodetector device with well suspended graphene microribbon contacted with Ti/Au metal contacts on both sides. (**c**) Schematic of the suspended graphene device during the photocurrent measurements.

The SEM image in **Figure 4b** shows a shadow underneath the graphene microribbon which indicates that it is fully suspended. We compared the device performance of the fully suspended graphene microribbon with the supported one. To avoid any influence of varying quality of the CVD graphene material or residual doping, we compared the same device before and after etching the sacrificial SiO_2 layer. The incident laser spot was scanned along the length of the graphene microribbon while recording the room-temperature photocurrent under V_{SD}=100 mV,

V_g=0 V, from the sample held in vacuum. The photocurrent contribution ΔI_{PC} from the graphene layer was corrected by subtracting the background value from the total recorded photocurrent values. **Figure 5** shows the photoresponse plotted against the laser position along the graphene microribbon for both cases. At the metal contacts, the photoresponse is sharply diminished compared to the photoresponse at the center of the 5 μm long microribbon. We attributed this dome-shape profile of the photocurrent to the particular Fermi-level bending at the Ti/graphene interface at both contacts. This behavior is similar to previous results with Ti/graphene interfaces at the contacts[12], which is in contrast to asymmetric profiles with positive and negative current contributions observed with Pt/graphene interfaces[26]. Most importantly, when comparing the peak values in the center, we observed a four-fold improved photoresponse in the fully suspended case.

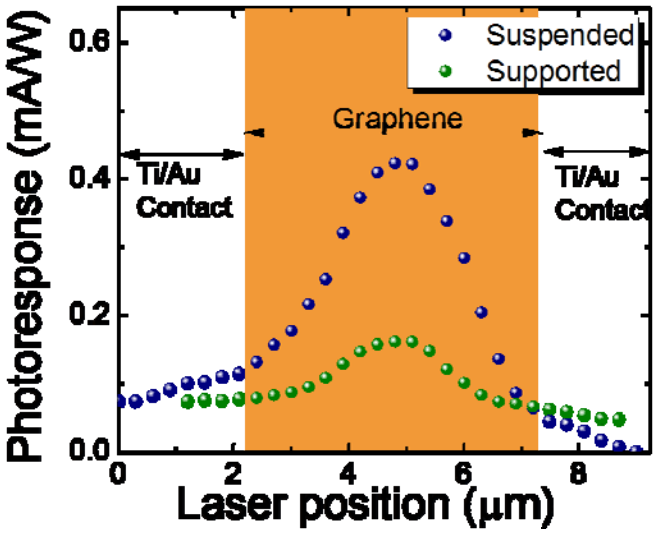

Figure 5. Spatial scans of photoresponse for substrate-supported (green dots) and suspended (blue dots) cases. The scan direction is along the length of the microribbon from contact to contact as indicated by the dashed line labeled "A" in Figure 2a. At the center position near 5 μm, a four-fold enhanced photoresponsitivity is found for the suspended graphene.

While demonstrating four-fold enhanced photocurrents in large-scale CVD-grown graphene photodetectors is of great technological importance, one would also like to understand the underlying photophysical mechanism to be able to optimize the detector device performance. The two main competing mechanisms for photocurrent generation in graphene are the photo-thermoelectric effect and the photoelectric effect. One way to tell these two effects apart is to characterize their time constant in optical pump-probe experiments which differ by at least an order of magnitude[26]. This technique requires, however, integration of our graphene microribbons into a coplanar stripeline circuit. In this study we showed that the slope of L-I curve is an alternative way to characterize the dominant mechanism for photocurrent generation. To this end the photocurrent was measured on a fully suspended graphene device and a fully supported one, respectively, under variable power, continuous-wave optical excitation. **Figure 6** shows the corresponding L-I curve on a logarithmic scale. Above the noise floor of

approximately 500 nW, the photocurrent I_{PC} rises nonlinearly with incident power (P_{opt}).

Ultimately, I_{PC} saturates at the highest pump power with values for suspended graphene being approximately 6-times smaller than those for supported graphene, as indicated by the arrow labeled "A" in Fig. 4. Above the noise floor and below saturation, the data follow a power law such that $I_{PC} \propto P_{opt}^{\alpha}$. For supported graphene we studied five different devices and found an

average value of $\alpha = 0.62 \pm 0.05$. In stark contrast, the power exponent of the fully suspended device is with 0.9, near unity. The pronounced change in slope of the L-I input-output curve indicates that the underlying physical mechanism has changed.

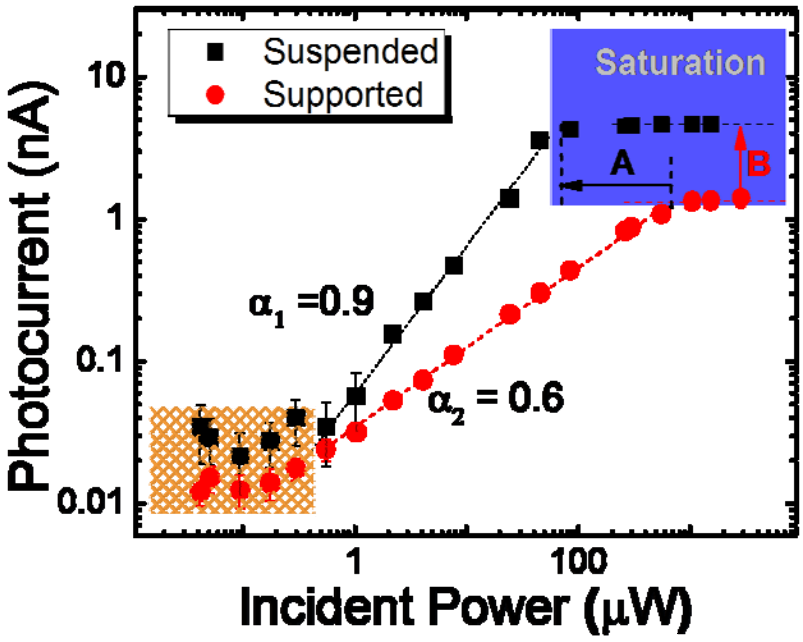

Figure 6. Light-current input/output curves. Photocurrent plotted against the incident laser power on a logarithmic scale showing enhanced photocurrent in the fully suspended graphene microribbons with significant slope change. The magnitude of the slope is indicative of the underlying photocurrent generation mechanism as detailed in the text. The black arrow (label A) indicates six-fold lower pump power levels for photocurrent saturation in the case of suspended graphene. The red arrow (label B) indicates four-fold increased photocurrents for suspended graphene in the saturation regime.

In summary, we have demonstrated fully-suspended chemical vapor deposition grown graphene microribbon arrays that are dominated by the faster photoelectric effect. Substrate removal has been found to enhance the photoresponse by four-fold compared to substrate-supported microribbons. Furthermore, we have shown that the light-current input/output curves give valuable information about the underlying photophysical process responsible for the generated photocurrent. These findings are promising towards wafer-scale fabrication of graphene photodetectors approaching THz cut-off frequencies.

REFERENCES

1. Xia, F., Mueller, T., Lin, Y.-M., Valdes-Garcia, A. & Avouris, P. Ultrafast graphene photodetector. *Nat. Nano* **4,** 839-843 (2009).

2. Xia, F. *et al.* Photocurrent imaging and efficient photon detection in a graphene transistor. *Nano Letters* **9,** 1039-1044 (2009)

3. Urich, A., Unterrainer, K. & Mueller, T. Intrinsic response time of graphene photodetectors. *Nano Letters* **11,** 2804-2808 (2011).

4. Ryzhii, V., Ryzhii, M., Mitin, V. & Otsuji, T. Terahertz and infrared photodetection using p-i-n multiple-graphene-layer. *J. Appl. Phys.* **107,** (2010).

5. Shi, Y., Fang, W., Zhang, K., Zhang, W. & Li, L.-J. Photoelectrical response in single-layer graphene transistors. *Small* **5,** 2005-2011 (2009).

6. Gu T. *et al.* Regenerative oscillation and four-wave mixing in graphene optoelectronics. *Nat. Photon.* **6,** 554-559 (2012).

7. Ju, L. *et al.* Graphene plasmonics for tunable terahertz metamaterials. *Nat. Nanotechnol.* **6,** 630-634 (2011).

8. Bao, Q. & Loh, K. P. Graphene photonics, plasmonics, and broadband optoelectronic devices. *ACS Nano* **6,** 3677-3694 (2012).

9. Bonaccorso, F., Sun, Z., Hasan, T. & Ferrari, A. C. Graphene photonics and optoelectronics. *Nat. Photon* **4,** 611-622 (2010).

10. Liu, M. *et al.* A graphene-based broadband optical modulator. *Nature* **474,** 64-67 (2011).

11. Sensale-Rodriguez, B. *et al.* Broadband graphene terahertz modulators enabled by intraband transitions. *Nat. Commun.* **3,** 780 (2012).

12. Mueller, T., Xia, F. & Avouris, P. Graphene photodetectors for high-speed optical communications. *Nat. Photon.* **4,** 297-301 (2010).

13. Xu, X., Gabor, N. M., Alden, J. S., van der Zande, A. M. & McEuen, P. L. Photo-thermoelectric effect at a graphene interface junction. *Nano Letters* **10,** 562-566 (2009).

14. Park, J., Ahn, Y. H. & Ruiz-Vargas, C. Imaging of photocurrent generation and collection in single-layer graphene. *Nano Letters* **9,** 1742-1746 (2009).

15. Freitag, M., Low, T., Xia, F. & Avouris, P. Photoconductivity of biased graphene. *Nat. Photon.* **7,** 53-59 (2013).

16. Lemme, M. C. *et al.* Gate-activated photoresponse in a graphene p–n junction. *Nano Letters* **11,** 4134-4137 (2011).

17. Peters, E. C., Lee, E. J. H., Burghard, M. & Kern, K. Gate dependent photocurrents at a graphene p-n junction. *Appl. Phys. Lett.* **97,** 193102-193103 (2010).

18. Song, J. C. W., Rudner, M. S., Marcus, C. M. & Levitov, L. S. Hot carrier transport and photocurrent response in graphene. *Nano Letters* **11,** 4688-4692 (2011).

19. Gabor, N. M. *et al.* Hot carrier–assisted intrinsic photoresponse in graphene. *Science* **334,** 648-652 (2011).

20. Sun, D. *et al.* Ultrafast hot-carrier-dominated photocurrent in graphene. *Nat. Nano* **7,** 114-118 (2012).

21. Liu, C. H., Dissanayake, N. M., Lee, S., Lee, K. & Zhong, Z. Evidence for extraction of photoexcited hot carriers from graphene. *ACS Nano* **6,** 7172-7176 (2012).

22. Graham, M. W., Shi, S.-F., Ralph, D. C., Park, J. & McEuen, P. L. Photocurrent measurements of supercollision cooling in graphene. *Nat. Phys.* **9,** 103-108 (2013).

23. Kim, R., Perebeinos, V. & Avouris, P. Relaxation of optically excited carriers in graphene. *Phys. Rev. B* **84,** 075449 (2011).

24. Low, T., Perebeinos, V., Kim, R., Freitag, M. & Avouris, P. Cooling of photoexcited carriers in graphene by internal and substrate phonons. *Phys. Rev. B* **86,** 045413 (2012).

25. Bistritzer, R. & MacDonald, A. H. Electronic cooling in graphene. *Phys. Rev. Lett.* **102,** 206410 (2009).

26. Prechtel, L. *et al.* Time-resolved ultrafast photocurrents and terahertz generation in freely suspended graphene. *Nat. Commun.* **3,** 646 (2012).

27. Konstantatos, G. *et al.* Hybrid graphene-quantum dot phototransistors with ultrahigh gain. *Nat. Nano* **7,** 363-368 (2012).

28. Sun, Z. *et al.* Infrared photodetectors based on CVD-grown graphene and PbS quantum dots with ultrahigh responsivity. *Adv. Mat.* **24,** 5878-5883 (2012).

29. Freitag, M., Low, T. & Avouris, P. Increased responsivity of suspended graphene photodetectors. *Nano Letters* **13,** 1644-1648 (2013).

30. Khomyakov, P. A. *et al.* First-principles study of the interaction and charge transfer between graphene and metals. *Phys. Rev. B* **79,** 195425 (2009).

31. Bao, W. *et al.* In situ observation of electrostatic and thermal manipulation of suspended graphene membranes. *Nano Letters* **12,** 5470-5474 (2012).

32. Chen, J.-H., Jang, C., Xiao, S., Ishigami, M. & Fuhrer, M. S. Intrinsic and extrinsic performance limits of graphene devices on SiO2. *Nat. Nano* **3,** 206-209 (2008).

33. Hwang, E. H. & Das Sarma, S. Single-particle relaxation time versus transport scattering time in a two-dimensional graphene layer. *Phys. Rev. B* **77,** 195412 (2008).

34. Rana, F. Electron-hole generation and recombination rates for Coulomb scattering in graphene. *Phys. Rev. B* **76,** 155431 (2007).

35. Du, X., Skachko, I., Barker, A. & Andrei, E. Y. Approaching ballistic transport in suspended graphene. *Nat. Nano* **3,** 491-495 (2008).

36. Bolotin, K. I. *et al.* Ultrahigh electron mobility in suspended graphene. *Solid State Commun.* **146,** 351-355 (2008).

37. Castro, E. V. *et al.* Limits on charge carrier mobility in suspended graphene due to flexural phonons. *Phys. Rev. Lett.* **105,** 266601 (2010).

38. Lindsay, L., Broido, D. A. & Mingo, N. Flexural phonons and thermal transport in graphene *Phys. Rev. B* **82,** 115427 (2010).

39. Seol, J. H. *et al.* Two-dimensional phonon transport in supported graphene. *Science* **328,** 213-216 (2010).

40. Wang, Z. *et al.* Thermal transport in suspended and supported few-layer graphene. *Nano Letters* **11,** 113-118 (2010).

PERSONNEL:

Eui-Hyeok Yang, Principal Investigator
Stefan Strauf, Collaborator
Vikram Patil, Graduate student
Kitu Kumar, Graduate student
Kyle Godin, Graduate student
Gabriella Shepard, Graduate student
Aaron Capone, Undergraduate student

PUBLICATIONS/ACCEPTED OR IN PRINT (partially or fully supported by this project):

Archival publications (published) during reporting period (partially or fully supported by this project):

1. V. Patil, K. Godin, S. Strauf and E. H. Yang, "Improved Photoresponse with Enhanced Photoelectric Contribution in Fully Suspended CVD Graphene Photodetectors" *Scientific Report* (2013)
2. K. Kumar, Y. Kim, X. Li, J. Ding, F. Fisher and E. H. Yang, "Chemical Vapor Deposition of Carbon Nanotubes on Monolayer Graphene Substrates: Reduced Etching via Suppressed Catalytic Hydrogenation Using C_2H_4," *Chemistry of Materials*, DOI: 10.1021/cm402052z (2013)
3. K. Kumar, K. Kim and E. H. Yang, "The Influence of Thermal Annealing to Remove Polymeric Residue on the Electronic Doping and Morphological Characteristics of Graphene," *Carbon*, 65, 35 (2013)
4. K. Kumar and E. H. Yang, "On the Growth Mode of Two-lobe Curvilinear Graphene Domains at Atmospheric Pressure," *Scientific Reports*, 3, 2571 (2013)
5. P. Hawkins, M. Begliarbekov, M. Zivkovic, S. Strauf, C. Search, "Quantum Transport in Graphene Ribbons with Realistic Edges," J. of Phys. Chem. C 116, 18382 (2012).

Conference Proceedings:

1. K. Kumar, Y.-S. Kim, Y. Tian, Andreas Pallikaras, and E. H. Yang, "The Effect of Thermal Annealing Processes on Graphene," Technical Proceedings of the 2013 NSTI Nanotechnology Conference and Expo, NSTI-Nanotech, National Harbor, Maryland, May 12-16, 2013.
2. Y.-S. Kim, K. Kumar, X. Li, F.T. Fisher, and E. H. Yang, "Fabrication and Characterization of 3-D Graphene-CNT Architectures Towards Supercapacitor Applications," *TechConnect World 2013 Conference and Expo*, National Harbor, Maryland, May 12-16, 2013.

Invited talks:

1. E. H. Yang, "Engineering Graphene and Carbon Nanotube Architectures for Sensing and Energy Storage Applications," Keynote*, International Conference and Exhibition on Laser, Optics and Photonics,* San Antonio, TX, Oct. 7-9, 2013.
2. E. H. Yang, "Nanoengineered Tunable Carbon Surfaces," *UKC 2013,* Newark, NJ, Aug. 7-9, 2013.

Changes in research objectives, if any: None

Change in AFOSR program manager, if any: Dr. Gernot Pomrenke (from Dr. James Hwang / Dr. Kitt Reinhardt)

Extensions granted or milestones slipped, if any: None

Include any new discoveries, inventions, or patent disclosures during this reporting period (if none, report none): None